ap

Asian Journal of Physics
Vol. 26, No 3 & 4 (2017) 171-180
Available on: www.asianjournalofphysics.in

Efficient hyperspectral target detection using class-associative spectral fringe-adjusted JTC with dimensionality reduction techniques

Paheding Sidike[1], Abduwasit Ghulam[1], Vijayan K Asari[2] and Mohammad S Alam[3]
[1]*Center for Sustainability, Saint Louis University, St. Louis, MO 63108, USA*
[2]*Department of Electrical & Computer Engineering, University of Dayton, Dayton, OH 45469, USA*
[3]*Department of Electrical Engineering & Computer Science, Texas A&M University-Kingsville, Kingsville 78363, Texas, USA*

Recent studies have shown that fringe-adjusted joint transform correlation (FJTC) can be effectively applied for single class and even multiclass object detection in hyperspectral imagery (HSI). However, directly utilizing FJTC based techniques for HSI processing may not be efficient due to the fact that HSI may contain a large volume of data redundancy. Therefore, incorporating dimensionality reduction (DR) methods prior to the object detection procedure is suggested. In this paper, we combine several DRs individually with class-associative spectral FJTC (CSFJTC), and then compare their performance on single class and multiclass object detection tasks using a real-world hyperspectral data set. Test results show that the CSFJTC with denoising autoencoder provides superior performance compared to the alternate methods for detecting few dissimilar patterns in the scene.

Keywords: Joint transform correlation (FJTC), Hyperspectral Imagery (HSI). Binary JTC (BJTC)

1 Introduction

Rapid advances in sensor technology increasingly provide great platform for developing many sophisticated object detection algorithms. For instance, most of the hyperspectral cameras today can provide hundreds to thousands of spectral bands to represent each pixel of interest. This dramatically improves the accuracy of object detection and characterization. Meanwhile, processing large volume of hyperspectral data poses challenges for researchers to extract useful information and to improve object detection performance in terms of accuracy and computational time.

In the past few decades, several efforts have been made to develop various object detection methods using Hyperspectral Imagery (HSI). The HSI-based object detectors can be categorized into two approaches: deterministic and probabilistic. Deterministic methods, such as spectral angle mapper [1], are comparably easy to implement since they usually do not require statistical modeling and estimation of target and/or background structures as probabilistic methods do; although probabilistic approaches may be more robust when considering noise effects. Therefore, developing more sophisticated methods for robust object detection using HSI is imperative.

Spectral Fringe-adjusted Joint Transform Correlation (SFJTC) [2], as a deterministic approach, has shown superior performance compared to alternates for detecting a set of similar patterns in HSI, while Class-associative SFJTC (CSFJTC) [3] is capable of detecting multiple dissimilar patterns simultaneously with single query from each class of pattern. It has also demonstrated that CSFJTC outperforms the state-of-the-art object detectors including both deterministic and probabilistic methods. Original concept of CSFJTC

Corresponding author:
e-mail: pahedings1@udayton.edu

is derived from Joint Transform Correlator (JTC) [4], which is one of the most successful optical correlators, has been widely used in many fields of studies [5-7]. JTC computes joint correlation of the input signal and the reference signal in the correlation plane in order to identify and localize targets of interest. One of the main merits of JTC is that it can be processed in real-time and does not require precise positioning. However, JTC suffers from broad correlation sidelobes and strong zero order peak [8-13]. To overcome the drawbacks of the classical JTC, a number of JTC variants have been proposed such as Binary JTC (BJTC) [8], Fringe-adjusted JTC (FJTC) [13], logarithmic FJTC (LFJTC) [14], rotation invariant FJTC [15], distortion-invariant FJTC [16], and phase-encoded FJTC [17]. Considering HSI-based object detection, techniques such as SFJTC, and its variants such as discrete wavelet transform SFJTC [18], logarithmic SFJTC [19] and CSFJTC have been proposed. In practice, CSFJTC may be more desirable since it can detect both single and multiple class objects using only one spectral signature from each class.

However, JTC-based techniques for HSI processing may not be effective or efficient for two reasons: 1) HSI usually contains a large volume of data redundancy and highly correlated bands that could affect the detection performance; 2) there exists interclass and intraclass spectral variations that could deteriorate pattern discriminability of a detector. Therefore, incorporating a preprocessing technique, such as dimensionality reduction (DR) methods prior to the object detection procedure is suggested [20, 21]. In this paper, we combine several DRs individually with CSFJTC, quantitatively analysis their performance, and then determine the contribution of DR methods for CSFJTC on object detection tasks in HSI.

The remainder of this paper is organized as follows. Section II reviews FJTC, SFJTC, CSFJTC and then introduces the proposed DR-based CSFJTC. Section III provides the experimental results and comparison. Finally, Section IV concludes this paper.

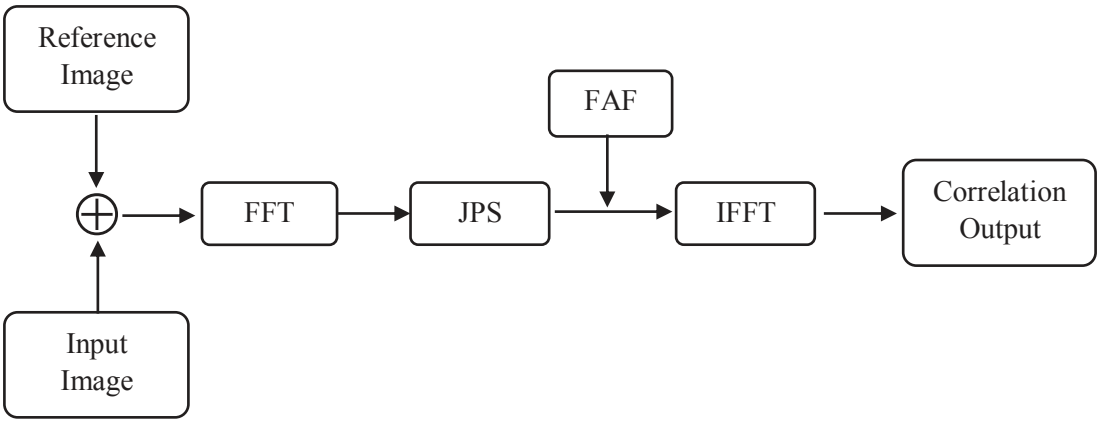

Fig. 1. Algorithmic flow of FJTC. FFT: Fast Fourier Transform; JPS: Joint Power Spectrum; IFFT: Inverse FFT; FAF: Fringe-adjusted Filter.

2 Theoretical Analysis

2.1 FJTC

A typical architecture of FJTC is depicted in Fig. 1. As shown in Fig. 1, FJTC contains the reference image and the input image, which are usually separated by a distance $2y_0$. If $r(x,y+y_0)$ denotes the reference image function, and $s(x,y-y_0)$ represents the input scene containing n objects $s_1(x-x_1,y-y_1)$, $s_2(x-x_2,y-y_2)$, … , $s_n(x-x_n,y-y_n)$, then the joint image function $f(x,y)$ can be expressed as

$$f(x,y) = r(x,y+y_0) + \sum_{i=1}^{n} s_i(x-x_i, y-y_i) \tag{1}$$

The Fourier transform of the input joint image function in the Fourier plane is written as

$$F(u,v) = |R(u,v)| \exp[j\phi_r(u,v) + jvy_0] + \sum_{i=1}^{n} |S_i(u,v)| \exp[j\phi_{si}(u,v) - jux_i - jvy_i] \quad (2)$$

where $|R(u,v)|$ and $|S_i(u,v)|$ are the amplitudes; $\phi_r(u,v)$ and $\phi_{si}(u,v)$ are respectively the phases of the Fourier transforms of $r(x,y)$ and $s_i(x,y)$, whereas u and v are mutually independent frequency domain variables. Accordingly, the joint power spectrum (JPS) is computed by

$$\begin{aligned} |F(u,v)|^2 &= |R(u,v)|^2 + \sum_{i=1}^{n} |S_i(u,v)|^2 \\ &+ 2\sum_{i=1}^{n} |S_i(u,v)| \, |R(u,v)| \cos[\phi_{si}(u,v) - \phi_r(u,v) - ux_i - vy_i - 2vy_0 \\ &+ 2\sum_{i=1}^{n} \sum_{\substack{k=1 \\ k\neq i}}^{n} |S_i(u,v)||S_k(u,v)|\cos\phi_{si}(u,v) - \phi_{sk}(u,v) - ux_i + ux_k - vy_i + vy_k] \end{aligned} \quad (3)$$

In Eq. (3), $|R(u,v)|^2$ are $|S_i(u,v)|^2$ are zero-order terms which produces additional autocorrelation between the targets and the reference. It is therefore suggested to use Fourier plane image subtraction (FPIS) [22] to eliminate the side effects. The FPIS can be achieved by subtracting the input-scene only power spectrum and the reference only power spectrum from $|F(u,v)|^2$, expressed as

$$\begin{aligned} C(u,v) &= |F(u,v)|^2 - |R(u,v)|^2 \\ &- \left\{ \sum_{i=1}^{n} |S_i(u,v)|^2 + 2\sum_{i=1}^{n} \sum_{\substack{k=1 \\ k\neq i}}^{n} |S_i(u,v)||S_k(u,v)| \times \cos[\phi_{si}(u,v) - \phi_{sk}(u,v) - ux_i + ux_k - vy_i + vy_k] \right\} \\ &= 2\sum_{i=1}^{n} |S_i(u,v)| \, |R(u,v)| \cos[\phi_{si}(u,v) - \phi_r(u,v) - ux_i - vy_i - 2vy_0 \end{aligned} \quad (4)$$

To avoid the pole problem associated with an inverse filter, Fringe-Adjusted Filter (FAF) [13] is applied to the resultant JPS in Eq. (4). FAF is defined as

$$H_{faf}(u,v) = \frac{B(u,v)}{A(u,v) + |R(u,v)|^2} \quad (5)$$

where $A(u,v)$ and $B(u,v)$ are either constants or functions of u and v. Finally, the FJTC correlation output is computed by inverse Fourier transform of the FAF transformed $C(u,v)$ as

$$\boldsymbol{c}(x) = F^{-1}\{\boldsymbol{C}(u,v) \times H_{faf}(u,v)\} \quad (6)$$

2.2 SFJTC

The diagram of SFJTC is shown in Fig. 2. The computational process of SFJTC is similar to FJTC. The main difference is that SFJTC computes on one-dimensional signal (e.g., one pixel in hyperspectral imagery) for each input sample, whereas FJTC operates on a two-dimensional image data as one input sample.

In addition, study in [2] proposed to use Peak-to-Clutter Mean (PCM) instead of Correlation Peak Intensity (CPI) to discriminate the targets from the background, because false signals may produce CPI that have very close value with that from true signals in the correlation plane. The PCM is defined as

$$\text{PCM} = \left(\frac{CPI}{L-1} \sum_{\tilde{c}_i \neq CPI} \tilde{c}_i(x) \right) \quad (7)$$

where L represents the half length of the correlation output vector. If the target presents in an unknown input image, the output of SFJTC in the half correlation plane will produce a high and sharp correlation peak at the location of the target in the scene.

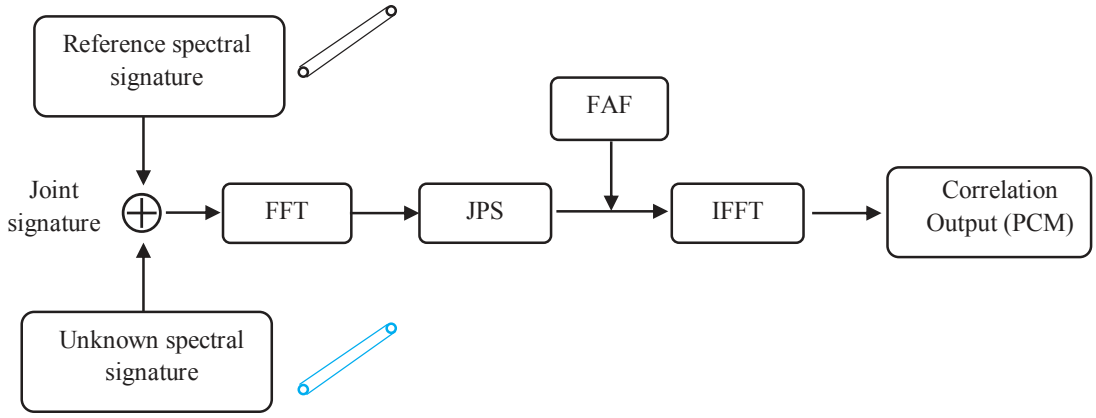

Fig. 2. Algorithmic flow of SFJTC. FFT: Fast Fourier Transform; JPS: Joint Power Spectrum; IFFT: Inverse FFT; FAF: Fringe-adjusted Filter; PCM: Peak-to-Clutter Mean.

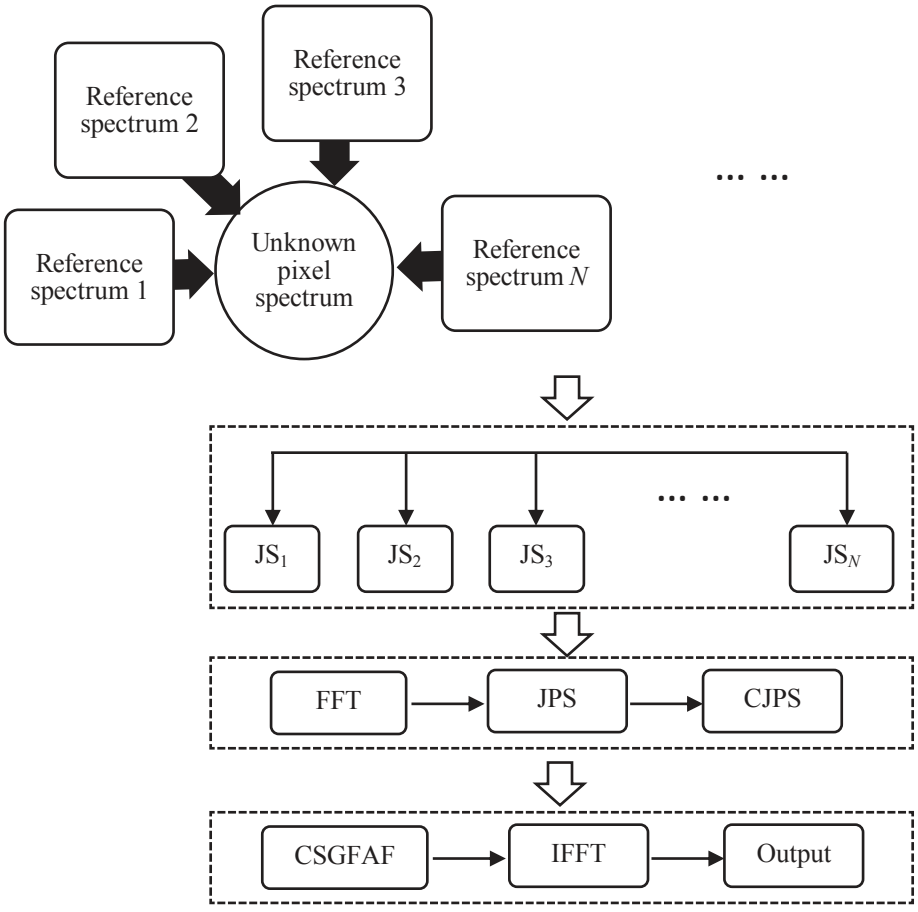

Fig. 3. Algorithmic flow of CSFJTC. JS: Joint Spectrum; FFT: Fast Fourier Transform; JPS: Joint Power Spectrum; CJPS: Combination of JPS; IFFT: Inverse FFT; CSGFAF: Class-associated Generalized Fringe-adjusted Filter.

2.4 CSFJTC

Figure 3 shows a block diagram of CSFJTC. The major difference between SFJTC and CSFJTC lies on the number of dissimilar input-reference-signal which accounts for the number of dissimilar patterns. Specifically, CSFJTC can handle multiple dissimilar patterns while SFJTC is designed only for detecting single class pattern. Consequently, the strategy for computing the joint signature is also different. In CSFJTC, the joint spectral signature is calculated separately for each reference spectrum. If we consider only two reference spectral signatures, denoted as $\boldsymbol{r}_1(x)$ and $\boldsymbol{r}_2(x)$, then the joint signatures are computed by Eqs. (8)-(11):

$$\boldsymbol{f}_{11i}(x) = \boldsymbol{r}_1(x+d) + \boldsymbol{s}_i(x-d) \tag{8}$$

$$\boldsymbol{f}_{21i}(x) = \boldsymbol{r}_1(x+d) - \boldsymbol{s}i(x-d) \tag{9}$$

$$\boldsymbol{f}_{12i}(x) = \boldsymbol{r}_2(x+d) + \boldsymbol{s}_i(x-d) \tag{10}$$

$$\boldsymbol{f}_{22i}(x) = \boldsymbol{r}_2(x+d) - \boldsymbol{s}_i(x-d) \tag{11}$$

where $\boldsymbol{s}_i = [s_{i1}, s_{i2}, \ldots, s_{iL}]$ represents the i^{th} ($i = 1,2,\ldots, M$) pixel spectrum when a hyperspectral dataset contains M pixels $\{s_i\}_{\text{i=1}}^{M}$, and the corresponding joint spectral signature is represented by $\boldsymbol{f}_i$. In the following steps, the fast Fourier transform is applied to Eqs. (8)-(11) separately and then JPS is computed. The removal of zero-order term is achieved by Eqs. (12) and Eqs (13):

$$\boldsymbol{P}_{1i}(u) = \boldsymbol{T}_{11i} - \mathbf{T}_{21i} = 4|\boldsymbol{R}_1(u)||\boldsymbol{S}_i(u)|\cos[\phi_{r1}(u) - \phi_{si}(u) + 2ud] \tag{12}$$

$$\mathbf{P}_{2\text{i}}(u) = \boldsymbol{T}_{12i} - \boldsymbol{T}_{22i} = 4|\boldsymbol{R}_2(u)||\boldsymbol{S}_i(u)|\cos[\phi_{r2}(u) - \phi_{si}(u) + 2ud] \tag{13}$$

where $\boldsymbol{T}_{11i}$, $\boldsymbol{T}_{21i}$, $\boldsymbol{T}_{12i}$, $\boldsymbol{T}_{22i}$ are the JPS of $\boldsymbol{f}_{11i}, \boldsymbol{f}_{21i}, \boldsymbol{f}_{12i}$, and $\boldsymbol{f}_{22i}$, respectively. To detect two classes of objects simultaneously, the JPS in (12) and (13) are further combined as

$$\begin{aligned}\mathbf{P}_i(u) &= a_1 \boldsymbol{P}_{1i}(u) + a_2 \boldsymbol{P}_{2i}(u) \\ &= a_1 \{4|\boldsymbol{R}_1(u)||\boldsymbol{S}_i(u)|\cos[\phi_{r1}(u) - \phi_{si}(u) + 2ud]\} \\ &+ a_2 \{4|\boldsymbol{R}_2(u)||\boldsymbol{S}i(u)|\cos[\phi_{r2}(u) - \phi_{si}(u) + 2ud]\}\end{aligned} \tag{14}$$

where a_1 and a_2 are constants which control the energy content of the input signal. Next, Class-associative Spectral Generalized FAF (CSGFAF) [3] is multiplied to $\boldsymbol{P}_i(u)$, that yields

$$\widetilde{G}_i(u) = \frac{[a_1 P_{1i}(u) + a_2 P_{2i}(u)]}{\epsilon + |R_1(u)|^m + |R_2(u)|^m} \tag{15}$$

where ϵ is a constant. The parameter m is a constant that may be either 0, 1 or 2. Finally, the CSGFAF filtered JPS is inverse Fourier transformed to obtain the correlation output. The detailed mathematical description of CSFJTC can be found in [3].

2.4 Proposed Scheme

In our proposed framework, four popular DR methods, which are Principal Component Analysis (PCA) [23], Probabilistic PCA (PPCA) [24], Denoising AutoEncoder (DAE) [25], and Factor Analysis (FA) [26], are individually combined with CSFJTC to perform object detection in HSI. All of these four DR methods are available in [27, 28]. The specific procedures are summarized as follows: the raw HSI is first sent to all four above mentioned DR methods separately while retaining first five components to extract useful

information, then the reference pixel signature from each class is randomly selected, finally the selected references and DR transformed data are fed into CSFJTC to perform the target detection task. A schematic of DR-based CSFJTC is depicted in Fig. 4.

3 Experiments and Discussion

The performance of four DR-based CSFJTC methods are examined using Area-Under-Receiver-Operating Characteristic (ROC) (AUROC). The AUROC describes the total area under ROC that is computed by the true positive rate as a function of the false positive rate. AUROC = 1 refers to the perfect detection, whereas AUROC<1 represents the possibility of a false positive detection. The parameters CSGFAF in CSFJTC were empirically set as $a_1 = a_2 = 0.5$, $\epsilon = 10^{-3}$ and $m = 2$. We also vary the number of components from 1 to 5 for all DR methods to investigate their effect on the detection outputs. In addition, the number for a dissimilar pattern is selected from {1, 3, 5}.

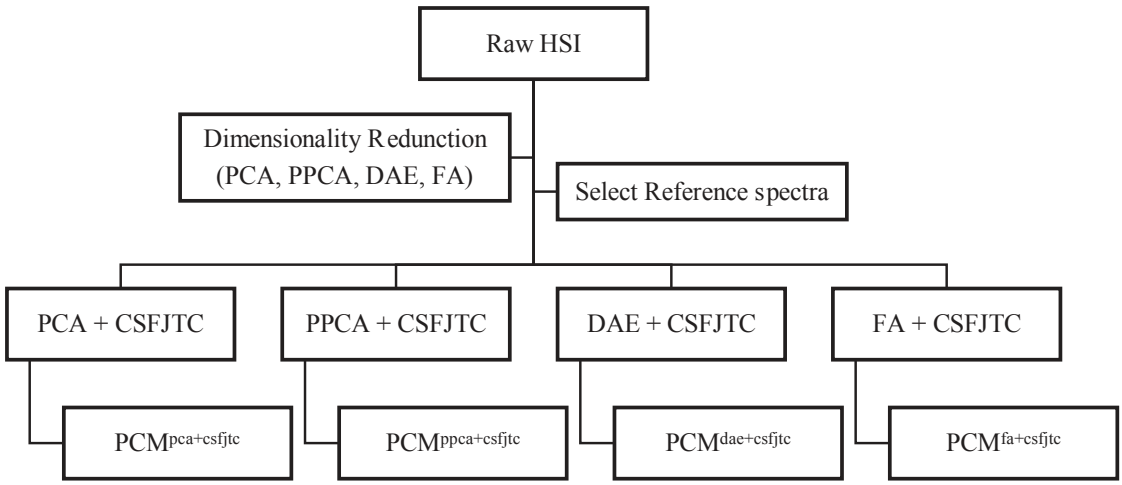

Fig. 4. DR-based CSFJTC for single/multiclass object detection.

3.1 Datasets

Salinas dataset [29]: This image was collected by AVIRIS over Salinas Valley, California. The data contains 224 spectral bands and each band has a size of 512×217 pixels with a spatial resolution of 3.7-meter per pixel. For better analysis, we removed twenty water absorption bands (108-112, 154-167, 224) before experiments, which results in 204 bands HSI. There are sixteen classes of targets contain in this image, including Brocoli, Fallow, Stubble, Celery, Grapes, Soil, Corn, Lettuce, Vinyard and their different types as shown in Fig. 5. Figs. 5 (a) and Fig 5 (b) show the corresponding false color composite image and ground truth data, respectively.

3.2 Results and Discussion

The experimental results are shown in Fig. 6 and Tables 1, 2, and 3. From Fig. 6, it can be observed that varying number of components (i.e., feature dimension) causes different detection accuracy for all DR methods. For instance, for three-class pattern detection, the AUROC of PCA-based CSFJTC is ranging from 0.6598 to 0.9340, which indicates that the number of feature dimension is a critical step. Furthermore, the values of AUROC tends to decrease when the targets contain more dissimilar patterns. This trend is especially obvious for DAE-based CSFJTC where AUROC is dropped from 0.9990 to 0.5655 if the number

of components is set to 5. This is because detecting more dissimilar patterns poses challenges to discriminate the pattern from the background and noise which may eventually affect the score of AUROC. Additionally, it is worth noting that DAE-based CSFJTC yields better results than the alternate methods for single-class and 3-class pattern detection, however, the performance is weakening when comes to detecting more dissimilar patterns.

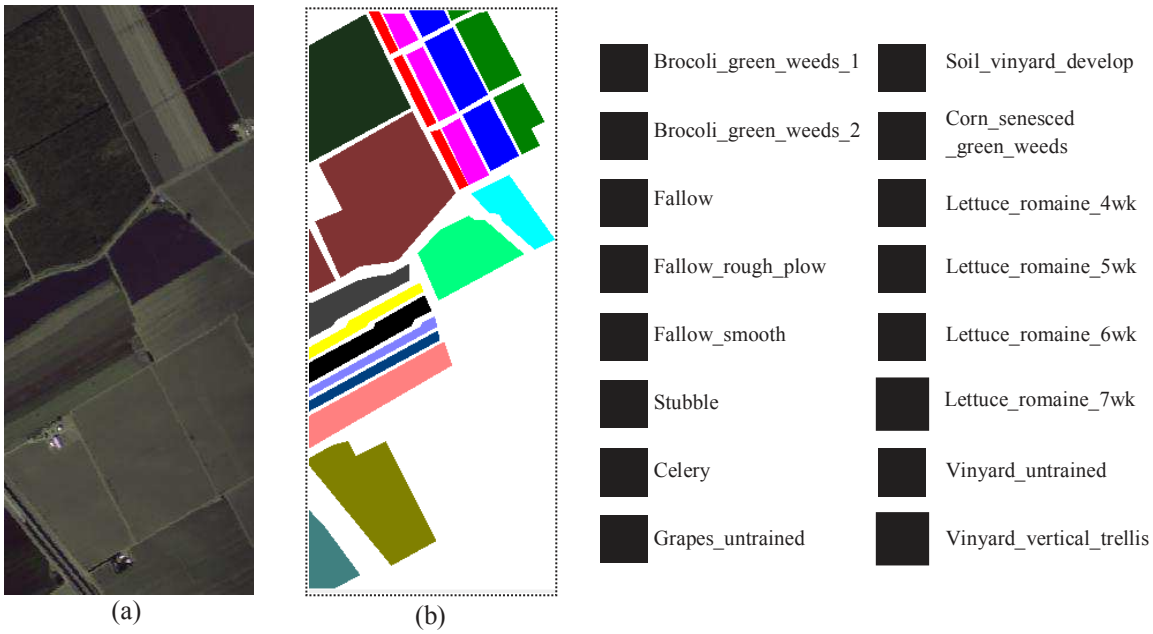

Fig. 5. The Salinas scene dataset. (a) False-color composite. (b) Ground truth

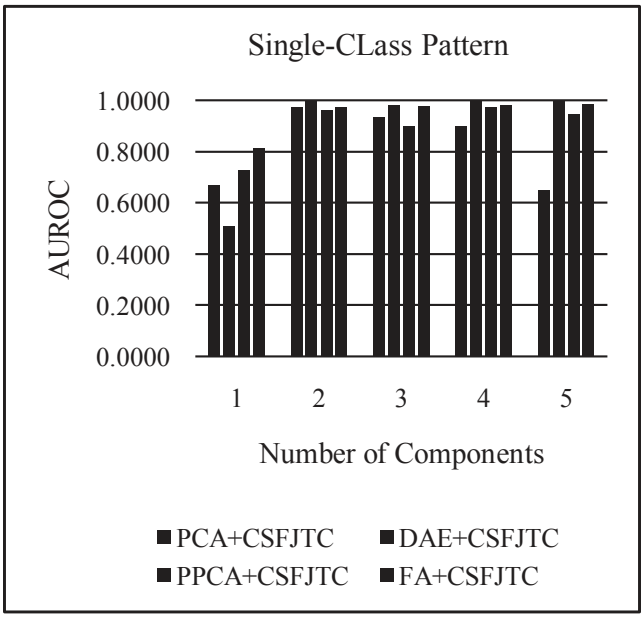

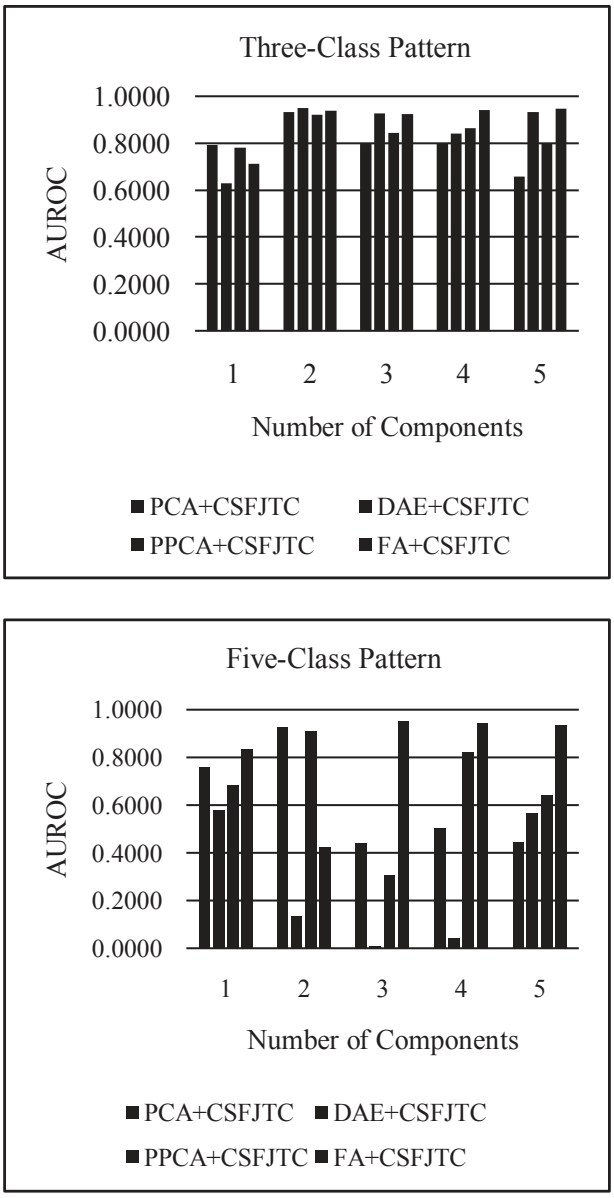

Fig. 6. Performance comparison using various number of components

Table 1. AUROC versus number of feature dimension for single class of object detection. The highest accuracy is marked in boldface.

Methods	Number of Feature Dimension				
	1	2	3	4	5
PCA+CSFJTC	0.6678	0.9727	0.9355	0.8979	0.6498
DAE+CSFJTC	0.5084	0.9983	0.9831	0.9984	**0.9990**
PPCA+CSFJTC	0.7264	0.9644	0.8958	0.9722	0.9448

FA+CSFJTC	0.8115	0.9738	0.9772	0.9826	0.9838
Spectral Only			0.9884		

Table 2. AUROC versus number of feature dimension for 3 classes of object detection.

Methods	Number of Feature Dimension				
	1	2	3	4	5
PCA+CSFJTC	0.7933	0.9340	0.8016	0.8005	0.6598
DAE+CSFJTC	0.6311	**0.9514**	0.9295	0.8413	0.9343
PPCA+CSFJTC	0.7811	0.9235	0.8463	0.8654	0.7994
FA+CSFJTC	0.7127	0.9386	0.9246	0.9413	0.9499
Spectral Only			0.7673		

Table 3. AUROC versus number of feature dimension for 5 classes of object detection.

Methods	Number of Feature Dimension				
	1	2	3	4	5
PCA+CSFJTC	0.7594	0.9291	0.4417	0.5029	0.4449
DAE+CSFJTC	0.5790	0.1349	0.0098	0.0426	0.5655
PPCA+CSFJTC	0.6848	0.9094	0.3085	0.8254	0.6409
FA+CSFJTC	0.8366	0.4252	**0.9534**	0.9440	0.9339
Spectral Only			0.5105		

One of the important aspects of introducing DR techniques to CSFJTC is to improve the detection performance. And it is evident that DR- based CSFJTC is superior compared to the spectral-only based CSFJTC in our experiments as shown in Tables 1-3. Especially for five-class pattern detection, we are able to achieve AUROC of 0.9534 while spectral-only method reaches only 0.5105. On the other hand, using less dimensional data obtained by DR, the computational speed can be potentially increased.

4 Conclusion

In this paper, we first provide a review of FJTC based pattern recognition techniques including FJTC, SFJTC and CSFJTC, and then introduce DR-based CSFJTC methods for single class and multiclass object detection frameworks. The evaluation is performed on the application to detect dissimilar patterns from HSI. Based on experimental results, it is concluded that DAE-based CSFJTC is robust for pattern discrimination when targets involve less dissimilar patterns. Also we observed that by varying the number of components in DR methods can yield different results which points out the significance of feature dimension for pattern detection. Therefore, developing a more advanced DR method for CSFJTC that are less sensitive to feature dimension will be our future research direction.

Acknowledgements

Funding for this work was supported by National Science Foundation (IIA-1355406), NASA (NNX15AK03H), and the Center for Sustainability at Saint Louis University.

References

1. Kruse F A, Lefkoff A B,J. Boardman W, Heidebrecht K B, Shapiro A T, Barloon P J,Goetz A F H, *Remote Sens*

Environ, 44(1993)145-163.

2. Alam M S, OchilovS , *Appl Opt*, 44 (2010) 18.Pl check and correct
3. Sidike P, Asari V J. Alam M S, *IEEE Trans Geosci Remote Sens*, 54(2016) 1196-1208;doi: 10.1109/TGRS.2015.2476480.
4. Weaver C S, Goodman J W, *Appl Opt*, 5(1966)1248-1249; doi.org/10.1364/AO.5.001248
5. Elbouz M, Alfalou A, Brosseau C, Yahia N B H, Alam M S, *Opt Commun*, 349(2015)65-82;doi.org/10.1016/j.optcom.2015.03.020
6. Vilardy J. M., Millán M. S., Pérez-Cabré E. Optics and Lasers in Engineering, 89 (2017) 88.
7. Sidike P., Alam M. S., Cui C., Asari V. K., *IEEE Proc. of Intl. Conf. on Adv. in Electrical Engineering*, (2013) 425.
8. Yu F. T. S., Song Q W, Cheng Y S, Gregory D A, *Appl. Opt*., 29 (1990) 225.
9. Javidi B., Kuo C, *Appl. Opt.*, 27 (1988) 663.
10. Yu F. T. S., Li C, Yin S, *Opt. Eng*., 37 (1) (1998) 52.
11. Tang Q, Javidi B, *Appl. Opt*., 32 (1993) 5079.
12. Johnson F. T. J., Barnes T H, Eiju T, Haskell T G, Matsuda K, *Opt. Eng*., 30 (12) (1991) 1947.
13. Alam M. S., Karim M A, *Appl. Opt*., 32(1993) 4344.
14. Sidike P, Alam M S, *Opt. Eng*., 52(2013) 103108.
15. Sidike P, Aspiras T, Asari V K, Alam M S, *Proc. SPIE: Optical Pattern Recognition Xxv*, 9094(2014) 90940F.
16. Sidike P, Asari V K, Alam M S, *Proc. SPIE: Image Processing: Machine Vision Appli. Vii*, 9024 (2014) 90240C.
17. Cherri A K, Alam M S, *Appl. Opt.* 40(2001)1216.
18. Sakla A., Sakla W., Alam M. S., *Appl. Opt.* 50(2011)5545.
19. Sidike P., Alam M. S., *SPIE Proc. of Conf. Defense, Security, and Sensing*, (2013) 87480T.
20. Sidike P., Chen C., Asari A., Xu Y., Li W., *IEEE Proc. of WISPERS, (2016)*.
21. Li W., Chen C., Su H. J., Du. Q., *IEEE Trans. Geosci. Remote Sens*., 30(2015) 3681.
22. Alam M. S., Karim M A, Opt. Eng., 33(1994) 1610.
23. Pearson K, *Philiosophical Magazine*, 2(1901) 559.
24. Tipping M. E., Bishop C. M., *Journal of the Royal Statistical Society: Series B*, 61 (1999) 611.
25. Vincent P., Larochelle H., Bengio Y., and Manzagol P.-A., *In Proc. of the International Conference on Machine Learning*, (2008)1096.
26. Spearman C., *American Journal of Psychology*, 15(1904) 206.
27. Available at: https://lvdmaaten.github.io/drtoolbox/
28. Maaten L.J.P. van der, Postma E.O., and Herik H.J. van den., *Tilburg University Technical Report*, TiCC-TR 2009-005, (2009).
29. Available at: *http://www.ehu.eus/ccwintco/index.php?title=Hyperspectral_Remote_Sensing_Scenes*

[Received : ..... ; accepted:.....]